Natural Cellulose Fiber as Substrate for Supercapacitor

Zhe Gui,[†,⊥] Hongli Zhu,[§,⊥] Eleanor Gillette,[†] Xiaogang Han,[§] Gary W. Rubloff,[§] Liangbing Hu,[§,*] and Sang Bok Lee[†,‡,*]

[†]Department of Chemistry and Biochemistry, University of Maryland, College Park, Maryland 20742, United States, [‡]Graduate School of Nanoscience and Technology (WCU), Korea Advanced Institute of Science and Technology, Daejeon 305-701, Korea, and [§]Department of Materials Science and Engineering, University of Maryland, College Park, Maryland 20742, United States. [⊥]These authors contributed equally to this work.

ABSTRACT Cellulose fibers with porous structure and electrolyte absorption properties are considered to be a good potential substrate for the deposition of energy material for energy storage devices. Unlike traditional substrates, such as gold or stainless steel, paper prepared from cellulose fibers in this study not only functions as a substrate with large surface area but also acts as an interior electrolyte reservoir, where electrolyte can be absorbed much in the cellulose fibers and is ready to diffuse into an energy storage material. We demonstrated the value of this internal electrolyte reservoir by comparing a series of hierarchical hybrid supercapacitor electrodes based on homemade cellulose paper or polyester textile integrated with carbon nanotubes (CNTs) by simple solution dip and electrodeposited with MnO_2. Atomic layer deposition of Al_2O_3 onto the fiber surface was used to limit electrolyte absorption into the fibers for comparison. Configurations designed with different numbers of ion diffusion pathways were compared to show that cellulose fibers in paper can act as a good interior electrolyte reservoir and provide an effective pathway for ion transport facilitation. Further optimization using an additional CNT coating resulted in an electrode of paper/CNTs/MnO_2/CNTs, which has dual ion diffusion and electron transfer pathways and demonstrated superior supercapacitive performance. This paper highlights the merits of the mesoporous cellulose fibers as substrates for supercapacitor electrodes, in which the water-swelling effect of the cellulose fibers can absorb electrolyte, and the mesoporous internal structure of the fibers can provide channels for ions to diffuse to the electrochemical energy storage materials.

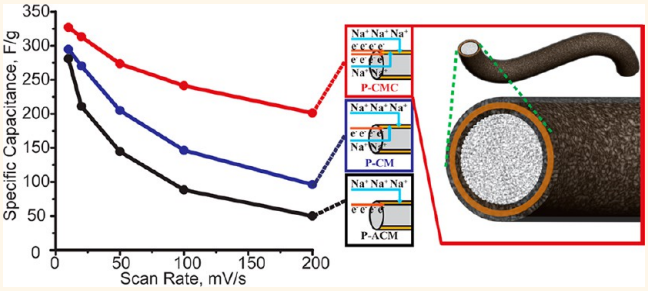

KEYWORDS: cellulose fibers · electrolyte absorption · carbon nanotubes · manganese oxide · supercapacitors · ion diffusion · electron transfer

During the past century, increasing attention and efforts have been devoted to the development of alternative energy sources and energy storage devices due to the urgent need to replace rapidly consumed fossil fuels and alleviate the climate change problem. To make the renewable and volatile energy produced from sun and wind feasible in daily use, we need viable storage devices to carry and deliver the energy. One field of great potential is supercapacitors, which provide high power and good cyclability. The charge is stored in a supercapacitor in two ways, a nonfaradic double-layer electrostatic charging process and a faradic surface redox process. Popular materials explored in this field include high surface area carbon materials, transition metal oxides, and conductive polymers.[1−4] During the charge/discharge process, the rates of electron transfer and ion diffusion directly affect the supercapacitors' performance.[5] For certain energy materials, such as MnO_2, approaches to facilitate the charge transfer processes include synthesizing composite components for better electrical conductivity as well as modification of the active material's structure to produce shorter diffusion lengths.[6−10] In our previous work, we have successfully engineered and synthesized MnO_2/poly(3,4-ethylenedioxythiophene) (PEDOT) coaxial nanowires and MnO_2 nanoparticle-enriched PEDOT nanowires, both of which effectively enhance the electrical conductivity by incorporating the conductive polymer PEDOT.[11−13] Some work has also been devoted to solving the ion diffusion issue by using different substrates like mesoporous carbon, carbon nanofiber,

* Address correspondence to binghu@umd.edu, slee@umd.edu.

Received for review April 12, 2013 and accepted June 18, 2013.

Published online June 18, 2013
10.1021/nn401818t

© 2013 American Chemical Society

graphite nanoplatelets, nanoporous gold, and conductive nanotubes for the synthesis of high surface area structures with shortened diffusion pathways for ions.[14−19]

Cellulose is an abundant and renewable raw material, suitable for industrial manufacturing. Cellulose and its derivatives have been applied to many aspects of our life for over 150 years and have been used for recent applications in fields such as electronics, biomaterials, and pharmaceuticals, where cellulose structure and properties have been found to be valuable.[20−24] Cellulose is well-known as the main component of the plant cell wall, which permits the passage of nutrients like water, ions, and small molecules, and maintains the cell shape with strong tensile strength. These attractive properties can also be applied to "energy cells". The native cellulose fibers applied here function like a cell wall that uptakes electrolyte from the bulk electrolyte bath. Electrolyte, like nutrients to the energy-active materials, is then transported *via* the pores through the matrix of cellulose fiber to the active materials. In this way, the mesoporous channels inside the fibers act as an extra ion diffusion pathway for the charge/discharge processes. Previously, porous cellulose fibers have been applied as a template for the synthesis of noble metal nanoparticles less than 10 nm,[25] and different wood tissues have been utilized to grow zeolites, demonstrating the mesoporous structure of the cellulose fibers.[26]

Here, we carried out a series of experiments using MnO_2 as the active material. We chose MnO_2, a very popular material for supercapacitors, because of its low cost, natural abundance, and environmental benignity. Both cellulose fibers (termed as "paper") and polyester fibers (termed as "textile") with and without electrolyte-blocking alumina coatings were used as the substrates for the deposition of MnO_2 to study the electrolyte absorption effect on supercapacitor performance. CNT wrapping was applied onto those substrates before electrodeposition to provide electrical conductivity. Results show that MnO_2 on the cellulose fiber substrate has improved electrochemical performance compared to the ones on Al_2O_3-blocked fibers. This is attributed to the extra electrolyte uptake through the porous fibers, but textile fibers lack the capability to act as an electrolyte reservoir like in paper fibers, which will be shown. Further optimization of the supercapacitor electrode was realized by coating the electrode paper/CNTs/MnO_2 with another CNT layer on top to enable the delivery of electrons to all the active materials.[16] Therefore, in the electrode with the configuration of paper/CNTs/MnO_2/CNTs (P-CMC), dual ion diffusion and electron transfer paths were enabled, resulting in high capacitance and good rate capacity. In this work, we have experimentally demonstrated the scientific significance of electrolyte absorption inside the cellulose fibers of paper for the application in supercapacitor substrates.

RESULT AND DISCUSSION

Cellulose Fiber Structure. Natural cellulose fibers are made of multiple individual macrofibrils, which are in turn composed of microfibrils which result from aggregation of the cellulose glucan chains. These chains are stabilized by the hydrogen bonds and van der Waals forces between the hydroxyl groups on the D-glucose units, resulting in regions with both amorphous and crystalline character.[27,28] Figure 1a shows the surface morphology of bare cellulose fiber. The network of microfibrils can be clearly identified. A cross section of a single fiber (indicated by the half-circle area) is shown in Figure 1b. In the corresponding high-magnification image (Figure 1c) of the red-squared area, the ends of the microfibrils that comprise the fiber, voids, and pores between fibrils are visible. The mesoporous structure of each fiber can be seen from the SEM image in Figure 1d. Pores are formed as voids between neighboring rod-like cellulose microfibrils that are packed in a parallel pattern mainly along the fiber axis. The pore size in the fiber is measured to be around 10−20 nm, as shown in the size distribution histogram in Figure 1d. It was reported that the cellulose fiber has a high specific surface area of 230 m^2/g accessible for water sorption.[29] Due to the pores and voids inside each fiber and the hydrophilic groups (hydroxyl group) along the cellulose chains, cellulose fibers can absorb water very well. When fully wetted, cellulose can take up to 140 wt % water inside the fibers as measured by the pulsed gradient spin−echo method.[30] When swollen in the aqueous electrolyte, all the pores in the fibers are open compared to the dry state, in which pore closure happens due to hydrogen bonding between adjacent microfibrils.[31,32] This pore characteristic is ideal for providing channels for electrolyte uptake. Meanwhile, the electron-rich oxygen atoms of the polar hydroxyl and ether groups in cellulose can also interact with electropositive transition metal cations,[25] such as sodium ions, therefore favoring the absorption of the electrolyte ions. With all of these properties, cellulose fiber can provide good diffusion channels for electrolyte solution, enhancing ion transportation to the active material. As a result, better electrochemical performance is to be expected. For comparison, we prepared cellulose fiber with blocked ion diffusion paths by coating a thin layer of alumina on the surface of the fiber using an atomic layer deposition (ALD) method. To highlight the advantage of cellulose fibers over other flexible substrates for electrolyte absorption, we also test polyester fibers with and without Al_2O_3 coating as substrates. SEM images of ALD-coated cellulose fiber and bare polyester fiber at the same magnification as Figure 1d are shown in Figure 1e,f, respectively.

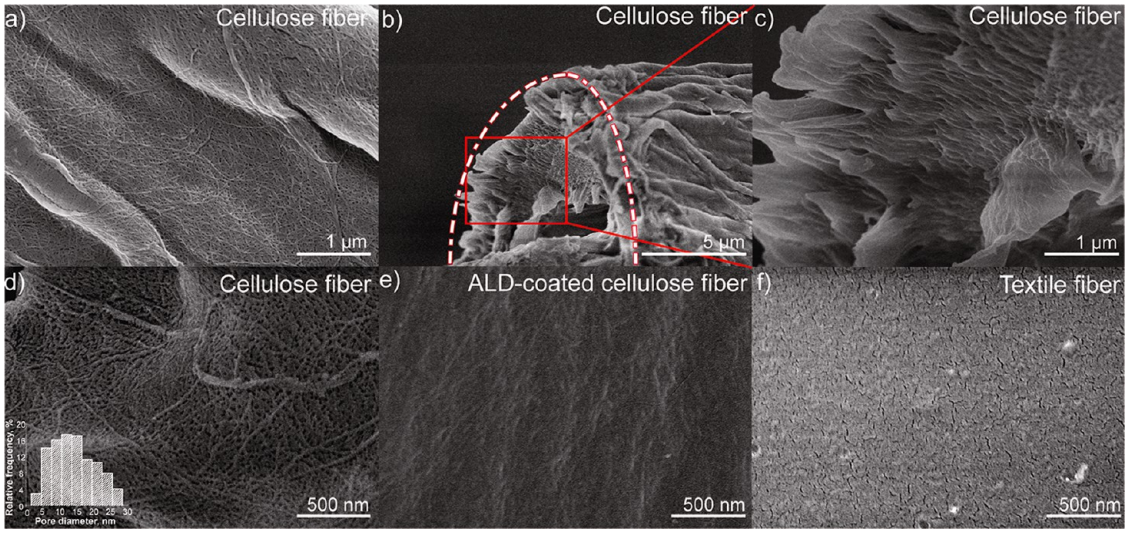

Figure 1. SEM images of the (a) surface and (b) cross section of a cellulose fiber. (c) SEM image of the framed area in (b). (d−f) SEM images at 50k magnification of the surfaces of a cellulose fiber, ALD-Al_2O_3-coated cellulose fiber, and a polyester fiber, respectively. All the fibers were sputtered with 2−5 nm gold to prevent localized charging and distortion. Inset of (d) shows the size distribution histogram of the pores in the cellulose fiber surface built by counting pores in the SEM image.

After ALD treatment, all the pores at the surface of the cellulose fiber are successfully blocked by the Al_2O_3 layer (compare Figure 1d to 1e). SEM image in Figure 1f (compare to Figure 1d) reveals the nonporous and relatively smooth surface morphology of polyester fiber. The small cracks observed in the image are due to the exposure of the electron beam.

Hybrid Electrode Preparation. We prepared a group of MnO_2 samples on these fiber substrates, engineered with either one or two ion diffusion pathways to study the effect substrates have on ion diffusion (see Table 1). An electrode with an additional CNT layer, paper/CNTs/MnO_2/CNTs (P-CMC), featuring dual diffusion paths for both ions and electrons was also prepared to demonstrate further optimized supercapacitive performance. Scheme 1 illustrates the preparation of electrode P-CMC. We started with a small piece of homemade paper prepared from Southern Yellow pine cellulose fibers using a vacuum filtration process. Conductive paper was prepared by dipping the paper into CNT ink, followed by drying in an oven.[33,34] We used an aqueous solution of manganese acetate and sodium acetate for the electrodeposition bath of MnO_2. After applying a constant potential of 0.65 V (*vs* Ag/AgCl), MnO_2 started to grow on the surface of the conductive paper and eventually formed a conformal thin layer (see Scheme 1b). The loading amount of the MnO_2 can be controlled by changing the charge passed during the electrochemical deposition. Another layer of CNTs was deposited on the top of MnO_2 afterward, as shown in Scheme 1d, by applying the same method used in step one. In Scheme 1e, we show the cross section of the configuration P-CMC and indicate the dual ion diffusion pathways (indicated by the red and blue curved arrows) and electron transfer pathways (indicated by the yellow and green straight arrows). For the ion diffusion process, besides the direct pathway 1 from bulk solution between each fiber to MnO_2, ions can also diffuse through path 2 from the inside of each water-absorbing cellulose fiber to MnO_2. Further improved capacitive performance of MnO_2 can be realized by wrapping the materials with another layer of CNTs on top to serve as a second electron transfer path for the MnO_2. Additionally, the top layer of CNTs functions as a protective layer to alleviate the loss of MnO_2 caused by the material's detachment from the fiber's surface during cycling.

TABLE 1. Summary of the Samples with Different Configurations

samples	configuration	ion path #	electron path #
P-CM	paper/CNTs/MnO_2	2	1
P-ACM	paper/Al_2O_3/CNTs/MnO_2	1	1
T-CM	textile/CNTs/MnO_2	1	1
T-ACM	textile/Al_2O_3/CNTs/MnO_2	1	1
P-CMC	paper/CNTs/MnO_2/CNTs	2	2

Electron microscopy was used to characterize fiber structure and the morphologies of deposited MnO_2 and CNTs layers. Figure 2a shows the CNT-paper before (left) and after (right) MnO_2 deposition. The area below the red dashed line in the right paper was immersed into the electrodeposition bath for MnO_2 growth. The SEM image of the CNT-paper (Figure 2b) shows clearly the CNT network layer covering and bridging between each fibril. This macroporous CNT layer will not influence the diffusion of electrolyte from the paper fibers underneath the MnO_2 deposited on top. The CNT-wrapped paper fibers were coated by a conformal MnO_2 layer (500−1000 nm in thickness) by

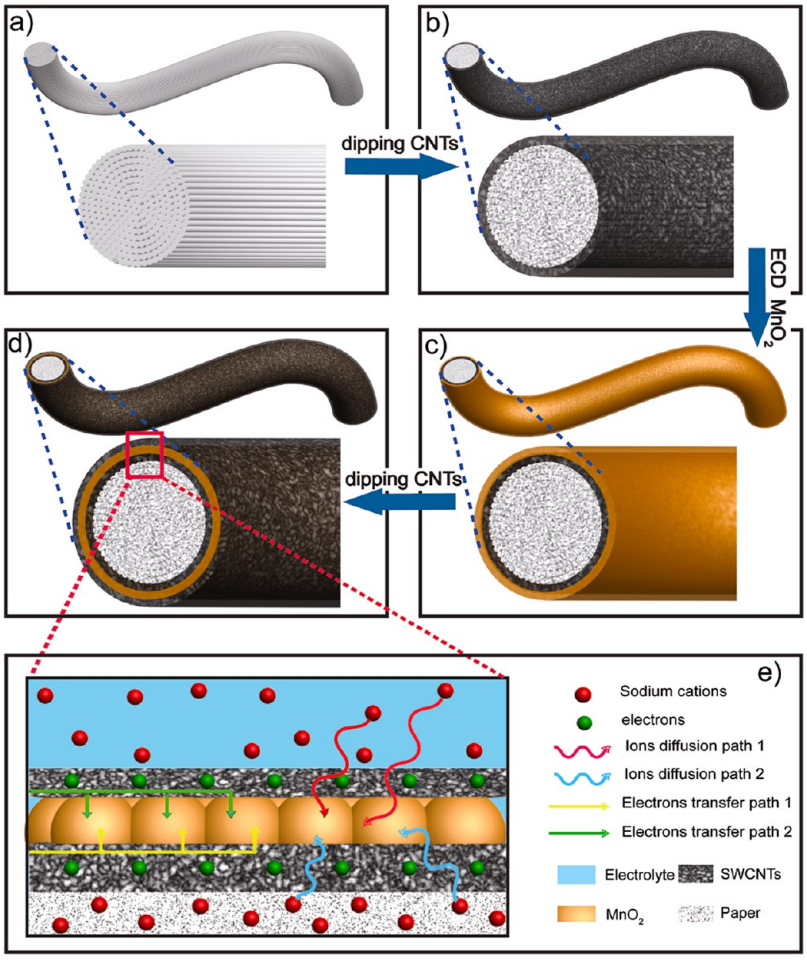

Scheme 1. Schematic illustration of the synthesis process. (a) One single cellulose fiber was used to illustrate the process. (b) CNT dip-coating. (c) Electrodeposition of MnO_2. (d) Second CNT dip-coating. (e) Magnification of the square area highlighted in (d) to illustrate the dual electron charge transfer and ion diffusion paths in the paper/CNTs/MnO_2/CNTs (P-CMC) configuration.

electrodeposition, forming the P-CM electrode. The corresponding high-magnification SEM image (Figure 2c) shows that the MnO_2 layer comprised petal-shaped nanoclusters in close arrangement, and each nanocluster was composed of nanosheets of a few nanometers in thickness.[35] This kind of architecture maximizes the surface area and facilitates the ion diffusion process. The electrodeposited MnO_2 has been characterized by Raman spectroscopy, as well, showing three major features at 503, 576, and 655 cm^{-1} that correspond to the Birnessite phase (see Supporting Information Figure S1).[36] The P-CMC electrode was produced by the addition of another CNT layer on top of the MnO_2. In the high-magnification SEM image (Figure 2d), we can clearly see the CNTs on the top as indicated by the red arrows (SEM images at higher magnification are provided in Figure S2). A cross-sectional view of the P-CMC sample prepared by microtome was also characterized by both SEM (Figure 2e) and TEM (Figure 2f). The red arrow in Figure 2e indicates the electrodeposited MnO_2 layer with a width around 1 μm at selected region. EDS mapping results of O and Mn further verify the location of the MnO_2 layer. The CNT layers on both sides of the MnO_2 are hard to observe due to the low contrast signals. However, due to the mechanical stress during the microtome sample preparation process, the MnO_2 layer detached from the fiber surface. In the void between the fiber surface and the MnO_2 layer, we can identify some individual CNTs and CNT bundles as indicated by the white arrow in Figure 2e. The same geometry was obtained by the TEM image in Figure 2f. A TEM image of MnO_2 at higher resolution is provided at bottom left. Some pairs of parallel line patterns can be identified in the image, presenting the cross section of the nanosheets that compose the MnO_2 layer with a width around 3 nm for each nanosheet (see Supporting Information Figure S3).

Electrochemical Characterization. To clearly verify the advantage of the additional ion diffusion pathway realized by the cellulose fibers, we compared the electrochemical performances of two samples in the configurations of paper/CNTs/MnO_2 (P-CM) and paper/Al_2O_3/CNTs/MnO_2 (P-ACM) (a schematic illustration can be found in Supporting Information Figure S4a).

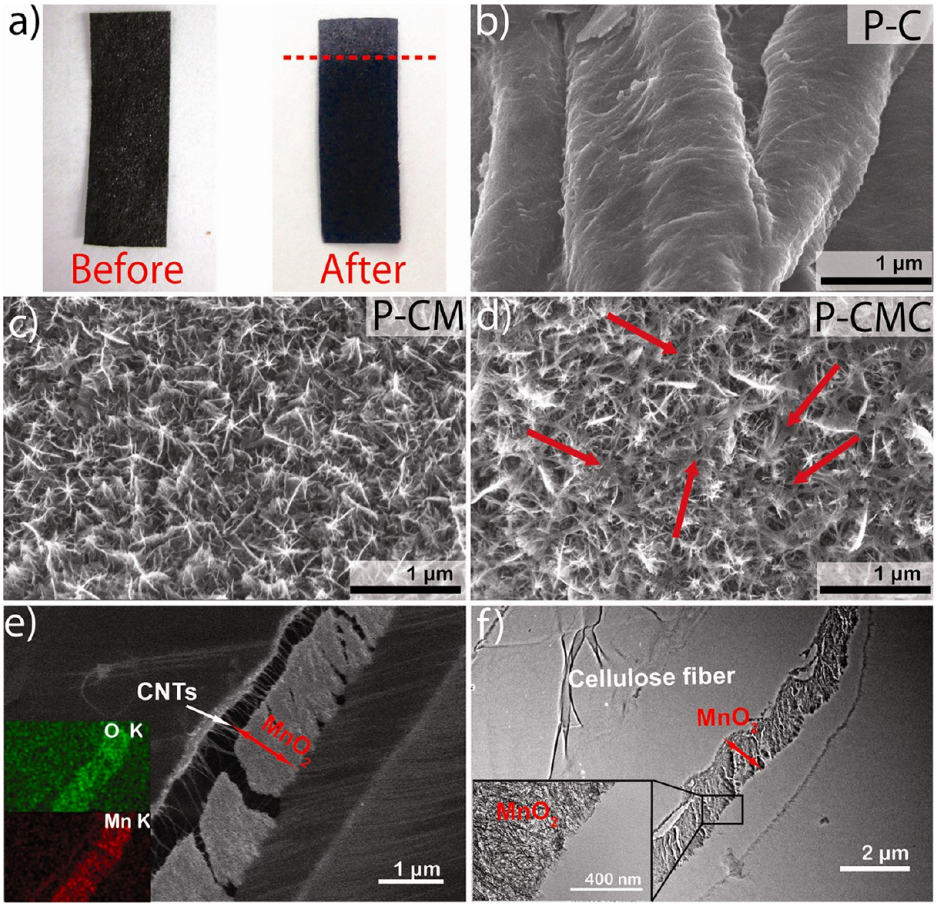

Figure 2. (a) Digital images of CNT-paper before (left) and after MnO_2 deposition (right). (b,c) SEM images of CNT-paper (P-C), paper/CNTs/MnO_2 (P-CM), and paper/CNTs/MnO_2/CNTs (P-CMC). Red arrows in (d) indicate the location of CNTs. (e) SEM and (f) TEM images of cross section of P-CMC prepared by microtome. Inset of (e) shows the corresponding EDS mapping of O (green) and Mn (red). Inset of (f) represents the TEM image of the framed area at higher magnification.

Paper fibers without Al_2O_3 coating have both ion diffusion paths, as indicated in Scheme 1e. However, for the paper fibers with Al_2O_3 coating (~17 nm), the pores on the surface of each cellulose fiber will be mostly blocked by the nonporous Al_2O_3 layer, preventing the fiber from absorbing electrolyte. Therefore, electrolyte can only access the space between each fiber but not inside the fiber. As a result, ions can only diffuse from the bulk electrolyte to MnO_2. Successfully coating of the Al_2O_3 layer was confirmed by the EDS mapping images of paper fibers coated with Al_2O_3 and CNT layers (see Supporting Information Figure S5). Additionally, we prepared samples in the same way, starting from a textile substrate composed of nonporous polyester fibers and wrapped with conductive CNTs (see Supporting Information Figure S4b). Therefore, the textile-based electrodes with or without an Al_2O_3 layer will both have only one ion diffusion path. This pair of textile-based samples demonstrates that the Al_2O_3 layer has no effect on electrochemical performance. The corresponding SEM images of a single fiber for P-ACM and T-ACM (textile/Al_2O_3/CNTs/MnO_2) electrodes are shown in Figure 3a,d, respectively. CNTs used in the electrode preparation for conductivity will also contribute to the double-layer capacitance out of the total capacitance. Therefore, electrochemical tests were also carried out on CNT-wrapped paper/textile samples without active MnO_2 (P-C, T-C), and the results are shown in Figure 3. The cyclic voltammetry (CV) curves for the two textile-based MnO_2 samples at 20 mV/s are shown in Figure 3e and demonstrate no difference. This means that the Al_2O_3 layer itself has no contribution to the capacitance and will not store any charge. For the paper-based samples, the CV curve of electrode P-CM shows a much more square shape than the P-ACM electrode (see Figure 3b), which can be attributed to the extra ion diffusion pathway in P-CM. In both paper and textile substrates, the capacitance contributions of the CNT layer are small (compare the green curve to the others in Figure 3b,e). The rate performances for the two samples of paper-based and of textile-based MnO_2 are shown in Figure 3c,f, respectively. Specific capacitances were calculated by subtracting the double-layer capacitance of the CNT layer estimated from the P-C/T-C electrodes. As the scan rate increases from 10 to 200 mV/s for the paper-based MnO_2 samples, the capacitance of electrode P-CM was maintained better than P-ACM. This is because the

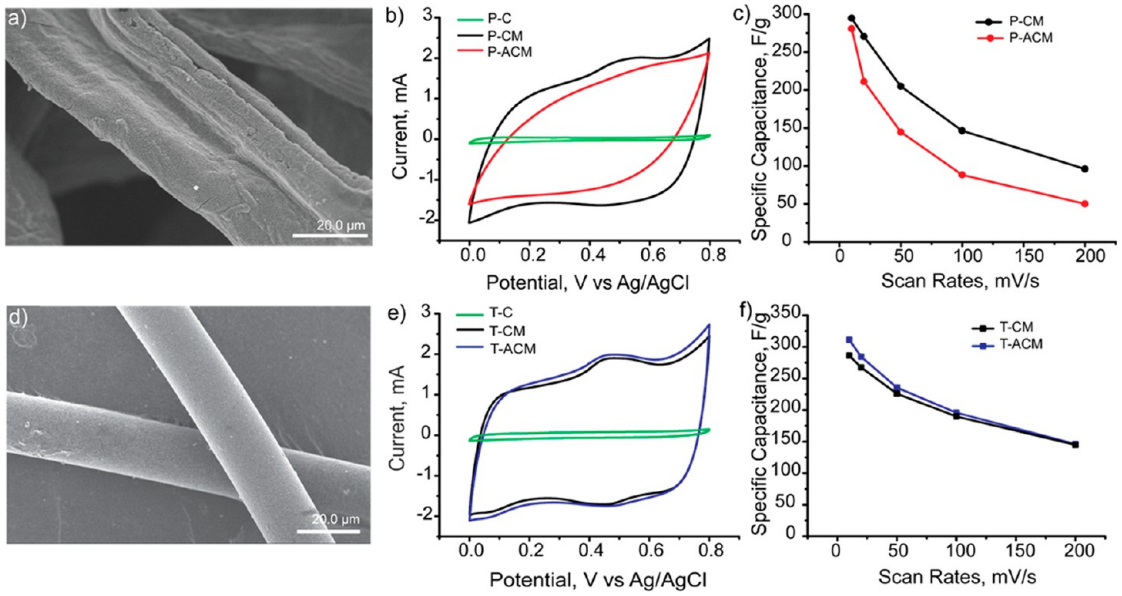

Figure 3. SEM images of Al_2O_3-coated (a) paper fibers and (d) textile fibers after MnO_2 deposition forming P-ACM and T-ACM, respectively. (b) Cyclic voltammetry curves of P-C (green), P-CM (black), and P-ACM (red) at 20 mV/s. (c) Specific capacitances of P-CM and P-ACM at different scan rates. (e) Cyclic voltammetry curves of T-C (green), T-CM (black), and T-ACM (blue) at 20 mV/s. (f) Specific capacitances of T-CM and T-ACM at different scan rates. The electrolyte in all experiments was 1 M Na_2SO_4.

higher scan rates require faster ion diffusion speed to access all the active material, and so, sample P-CM with better ion diffusion access can better utilize the MnO_2 and maintain specific capacitance at higher scan rates or current density than P-ACM. For comparison, the two textile-based samples show nearly identical capacitances even at higher scan rates. These results confirm that the ion diffusion process can be effectively boosted by using an electrolyte-absorbing cellulose paper substrate.

While performance can be improved by the double ion diffusion paths realized by the cellulose paper substrate, further optimization of the hybrid electrode can be achieved by doubling the electron paths, as well. By simply wrapping the P-CM electrode with one extra layer of CNT coating on the top, we produced electrodes in the configuration of paper/CNTs/MnO_2/CNTs (P-CMC). Both P-CMC and P-CM have two ion diffusion paths but different electron transfer path numbers. As illustrated in Scheme 1e, the P-CMC sample with two CNT layers provides two electron transfer paths for the active materials while sample P-CM has only one electron transfer path. The cyclic voltammetry (CV) curves at 50 mV/s in Figure 4a show that sample P-CMC had a more square shape CV curve than the electrode P-CM, which indicates better capacitive performance, as is expected from a supercapacitor with higher conductivity. Specific capacitances at different scan rates from 10 to 200 mV/s for the two samples are shown in Figure 4b. MnO_2 has poor conductivity of 10^{-5}–10^{-6} S cm^{-1}, so electron transfer will limit the capacitance especially at high scan rates. Therefore, the P-CM sample demonstrates significantly

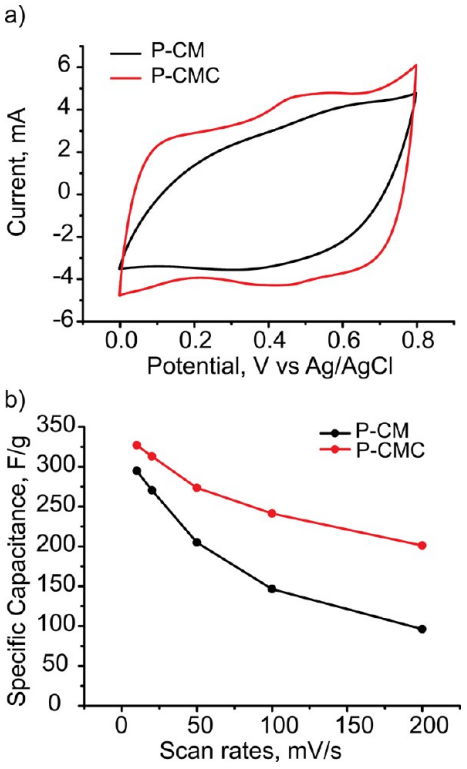

Figure 4. (a) Cyclic voltammetry curves of P-CM (black) and P-CMC (red) at 50 mV/s in 1 M Na_2SO_4 electrolyte. (b) Specific capacitances of P-CM (black) and P-CMC (red) at different scan rates in 1 M Na_2SO_4 electrolyte.

worse rate performance, with the specific capacitance value dropping from 295 F/g at 10 mV/s to only 96 F/g at 200 mV/s (32.5% maintained).The P-CMC sample shows much better rate performance as well as a higher initial specific capacitance. The dual electron

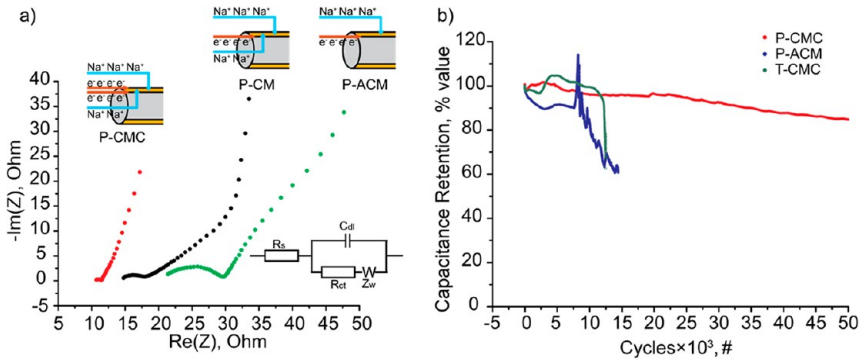

Figure 5. (a) Nyquist electrochemical impedance spectra of three samples: P-CMC (red), P-CM (black), P-ACM (green) measured in 1 M Na_2SO_4 under open circuit voltage conditions. Ion diffusion paths are presented by the blue arrows, and electron transfer paths are indicated by the red arrows in the cartoons. Inset of (a) shows the equivalent circuit. (b) Cycling performance of P-CMC (red), P-ACM (blue), and T-CMC (green) at 3 mA/cm^2 in 1 M Na_2SO_4 electrolyte for up to 50k cycles.

pathways in the P-CMC sample result in specific capacitance of 327 F/g at scan rate of 10 mV/s and 201 F/g at 200 mV/s (61.5% maintained). The amount of CNTs coated on the paper can be controlled by changing the dip and dry procedure repeating times. In this work, we dipped only one time for the second CNT layer, but it is possible that even better rate performances could be achieved by optimizing the dipping times of the CNT layers.

Electrochemical Impedance Spectra. To further study the charge transfer resistance in the paper-based MnO_2, electrochemical impedance spectroscopy results from three different samples were collected and compared, as shown in Figure 5a. The P-CMC sample was compared to the P-CM sample without the second electrical pathway as well as the P-ACM sample with only one electrical and one ionic diffusion pathway to demonstrate the effect of each aspect of this design on charge transfer resistance (see Table 1 for sample configurations). At high frequency, the intercept of the real axis represents the equivalent internal resistance (R_s), which includes the electrolyte resistance, intrinsic resistance of the active materials, and contact resistance at the interface between the current collector and the active materials. The R_s for the sample P-ACM was 21.4 ohm. This value was higher than the 15.7 ohm of sample P-AC because of the nonconductive Al_2O_3 layer deposited onto the fiber surface. For sample P-CMC, an even lower R_s value of 10.7 ohm was obtained, which can be attributed to the extra conductive CNT layers. At the medium−high frequency range, all three curves show well-defined semicircles. The diameter of the semicircles corresponds to the charge transfer resistance (R_{ct}) at the interface where faradic reaction takes place, involving both ion and electron transfer processes. The R_{ct} value was lowest for the sample P-CMC (0.7 ohm) with dual charge transfer paths for both electrons and ions and highest for sample P-ACM (8.2 ohm) with only one path for electron transfer and ion diffusion. From our simple model (as illustrated in Scheme 1e), the charge transfer resistance of P-CM with both sides of the MnO_2 layer accessible for ion insertion/desertion should be around 50% of the value of P-ACM, which has only one side that has been used for ion diffusion due to the Al_2O_3 blocking. The charge transfer resistance measured from EIS is 3.2 ohm for sample P-CM, which is approximately half the value for sample P-ACM blocked by Al_2O_3. The deviation from exactly 50% may be due to the sample preparation variation and the limited transport of electrons. At high frequency, both P-CMC and P-CM electrodes show a nearly 90° linear region, which indicates the ideal capacitor behavior, while for P-ACM, the EIS curve deviates much more with an angle from the vertical line.[37,38] This result further confirms that more electron transfer and ion diffusion paths are provided within the configuration of P-CMC, and the internal resistance and charge transfer resistance are effectively reduced.

Cycling Performance of P-CMC. Figure 5b shows the cycling performance of three electrodes evaluated by galvanostatic charge/discharge at current density of 3 mA/cm^2 for up to 50 000 cycles. For the first few hundred cycles, the specific capacitance of all three electrodes dropped by around 4%. For both P-CMC and T-CMC electrodes, the curves show increasing capacitance retention up to 3000th and 5000th cycles, respectively. This phenomenon can be attributed to the complete electrolyte wetting effect of the cellulose and polyester fibers over time. As paper/textile became saturated by the electrolyte, faster ion diffusion process was enabled. Polyester textile can only be wetted between fibers, while cellulose paper can absorb water very well inside each fiber due to its excellent nature of hydrophilicity. Therefore, the saturated point appeared earlier for the P-CMC (at the 3000th cycle) than the T-CMC (at the 5000th cycle). The capacitances for both electrodes started to decrease after the saturated points, a change which is likely due to the dissolution of MnO_2 into the electrolyte after long-time cycling.[9] T-CMC showed fast capacitance decay from the 10000th cycle and maintained only 62% capacitance at the 12500th cycle. For P-CMC, much better

capacitance retention was reached with 96, 93, 88, and 85% capacitance retentions at the 20000th, 30000th, 40000th, and 50000th cycles, respectively. This longer cycling life of MnO_2 deposited on cellulose fibers than on polyester fibers is likely due to the fibers' different surface roughness. For polyester fiber with a relative smooth surface, the MnO_2 layer peeled off easier. For cellulose fiber with a more rough surface geometry, the MnO_2 stuck to the substrate better and survived a longer cycling test. For the P-ACM electrode, the electrolyte wetting was prevented by the ALD layer blocking at first. When it came to around the 8000th cycle, the capacitance increased suddenly, which can be explained by the breaking of the Al_2O_3 layer after thousands of cycles and following electrolyte wetting of the fibers that were exposed to the bulk solution. Due to the breaking of the ALD layer, it started to peel off from the fibers together with the MnO_2 deposited above. Therefore, we see quick decay of the capacitance of P-ACM afterward. The cycling performance of P-CMC achieved in this work shows much better capacitance retention than many of the previously reported MnO_2 retention capabilities, improving on reported performances of 75−90% for up to 2000 cycles.[39,40] The P-CMC electrode also survived a much longer cycling life at similar capacitance decay rate compared that reported by Bao *et al.* for the MnO_2 deposited on conductive polyester textile fibers, which showed good capacitance retention around 95% over 3000 cycles at a current density of 1 mA/cm^2.[16]

CONCLUSION

In summary, we use cellulose fibers with a porous internal structure as the substrate for the deposition of electrochemical energy storage materials to facilitate the ion diffusion process. Different substrates, either with or without open pores, were studied for comparison, and results show that cellulose fibers with open pore channels extending along the fiber gave better electrochemical performance, which can be attributed to the extra ion diffusion pathway realized through the electrolyte uptake by the cellulose fibers. Further improved electrochemical performance can be achieved by applying an additional conductive wrapping of CNTs on the surface of P-CM, resulting in configuration of P-CMC. In this P-CMC electrode, dual ion and electron paths are realized and provide even better capacitive performance. The cellulose-paper-based substrate also shows excellent cycling performance, retaining 85% of its capacitance up to 50k cycles. This work was able to demonstrate the specific advantages of improved ion pathways that can be provided by a mesoporous cellulose fiber substrate and its substantial potential for other energy materials as well in energy device design.

EXPERIMENTAL SECTION

Conductive Paper Preparation. Native cellulose fiber (170 mg) disintegrated from Southern Yellow pine was added to 340 mL of distilled water and stirred with IKA RW20 digital mixer at 700 rpm for ∼20 min. A uniform fiber suspension was obtained and poured into a Buchner funnel with fritted discs for vacuum filtration. A wet sheet was formed in ∼3 min and dried in an oven at 100 °C for 5 min. The whole process is water-based and additive-free. Textile composed of polyester fibers was commercially available from Walmart. P3 SWNTs were purchased from Carbon Solutions (California). CNTs (10 mg) were added to 10 mL of DI water with 1% SDBS, followed by 5 min bath sonication, 3 min probe sonication, and centrifugation purification. Then 1 mg/mL SWNT ink was prepared. The lab-made paper/textile sheet was dipped in the CNT ink for 2−3 min and dried in an oven at 100 °C. This procedure was repeated three times to achieve a resistance around 30 ohms (measured by a four-point probe technique (EDTM)). The conductive paper/textile was then rinsed with DI water to remove the residual surfactant. For Al_2O_3-coated paper/textile substrates, the ALD Al_2O_3 coating was performed in a commercial BENEQ TFS 500 reactor with a base pressure of 2 mbar. Trimethyl aluminum [TMA, $Al(CH_3)_3$] and DI water were used as precursors at 150 °C. After 240 cycle deposition, the thickness of the ALD Al_2O_3 is around 17 nm, estimated by measuring the thickness of ALD Al_2O_3 film deposited at the same condition on a silicon wafer using a N&K spectrophotometer.

Electrochemical Deposition of MnO_2 on CNT-Papers. First, the CNT-paper was cut into square pieces. The electrochemical deposition of manganese oxide was performed by using a three-electrode setup, where Ag/AgCl electrode was used as the reference electrode and platinum as the counter electrode. The working electrode was made of a piece of CNT-paper, which was sandwiched by two small pieces of platinum at one end and connected to an alligator clip to avoid side reaction that may occur at the alligator. Then CNT-paper was immersed in the aqueous electrolyte bath consisting of 20 mM manganese acetate and 100 mM sodium acetate. A constant potential of 0.65 V *versus* Ag/AgCl electrode was applied until the charge passed reached 600 mC. After the electrodeposition, the CNT-paper was rinsed with distilled water twice and dried in air at room temperature.

Characterization. The MnO_2-CNT-paper structure was investigated using a field emission scanning electron microscope (Hitachi SU-70 SEM, operated at an acceleration voltage of 5 keV) and a transmission electron microscope (JEM 2100 FE-TEM). The microtomed sample was mounted in Spur epoxy resin and cut with a Reichert Ultracut E Ultratome microtome with a diamond knife (Leica, Vienna, Austria) at room temperature.

Electrochemical Measurement. All the electrochemical studies were conducted in a standard three-electrode system using a bipotentiostat (BI-STAT; Princeton Applied Research). A platinum counter electrode was used in conjunction with a Ag/AgCl reference electrode for all the measurements. In order to calculate the specific capacitance of the MnO_2-CNT-paper, cyclic voltammetry at different scan rates (10−200 mV/s) was performed by cycling the voltage between 0 and 0.8 V in 1 M Na_2SO_4 solution. The specific capacitance was calculated from cyclic voltammograms based on the equation

$$C_{sp} = Q/\Delta Em$$

where the Q is the charge stored in the CV curve (charge stored by the double-layer capacitance of the CNT layer has been subtracted) and ΔE is 0.8 V, and m is the mass of MnO_2, calculated from the charge passed in the electrochemical deposition. Specific capacitances were calculated by subtracting the double-layer capacitance of the CNT layer estimated

from the P-C/T-C electrodes. We want to point out here that the double-layer capacitances of the CNTs in P-C/T-C will not necessarily equal the capacitance contribution of the CNTs in the composited electrodes. Double-layer capacitance is determined by the surface area, and the CNT-exposed surface area will become smaller after being covered by the MnO_2 layer. Here we use an approximate value for the calculation. Electrochemical impedance spectroscopy was also conducted in a three-electrode configuration, with a frequency range from 100 kHz to 100 mHz at open circuit potential.

Conflict of Interest: The authors declare no competing financial interest.

Acknowledgment. The work was supported by the Science of Precision Multifunctional Nanostructures for Electrical Energy Storage (NEES), an Energy Frontier Research Centre funded by the U.S. Department of Energy, Office of Science, Office of Basic Energy Sciences under Award Number DESC0001160. L.H. thanks the start up support from University of Maryland College Park as leverage for the NEES EFRC research. We thank P. J. Shang (NISP Lab) for assistance in TEM, and T. Maugel (Biological Ultrastructure Lab) for assistance in preparing the microtome sample.

Supporting Information Available: Raman spectra of MnO_2 deposited on conductive cellulose paper. SEM images of paper/CNTs/MnO_2/CNTs (P-CMC) at high magnification of 70 and 100k. TEM image of the MnO_2 layer in the microtomed cross section of sample P-CMC. Schematic illustration of the fabrication cellulose fibers and polyester fibers. SEM image and EDS mapping of C and Al on a segment of cellulose fibers coated with Al_2O_3 and CNT layers (paper/Al_2O_3/CNTs). This material is available free of charge *via* the Internet at http://pubs.acs.org.

REFERENCES AND NOTES

1. Naoi, K.; Morita, M. Advanced Polymers as Active Materials and Electrolytes for Electrochemical Capacitors and Hybrid Capacitor Systems. *Electrochem. Soc. Interface* **2008**, *17*, 44–48.
2. Naoi, K. New Materials and New Configurations for Advanced Electrochemical Capacitors. *Electrochem. Soc. Interface* **2008**, *17*, 34–37.
3. Simon, P.; Burke, A. Nanostructured Carbons: Double-Layer Capacitance and More. *Electrochem. Soc. Interface* **2008**, *17*, 38–43.
4. Bélanger, D.; Brousse, L.; Long, J. Manganese Oxides: Battery Materials Make the Leap to Electrochemical Capacitors. *Electrochem. Soc. Interface* **2008**, *17*, 49–52.
5. Conway, B. *Electrochemical Supercapacitors: Scientific Fundamentals and Technological Applications (POD)*; Kluwer Academic/Plenum: New York, 1999.
6. Liu, R.; Duay, J.; Lee, S. B. Heterogeneous Nanostructured Electrode Materials for Electrochemical Energy Storage. *Chem. Commun.* **2011**, *47*, 1384–1404.
7. Zhang, S. W.; Chen, G. Z. Manganese Oxide Based Materials for Supercapacitors. *Energy Mater.* **2008**, *3*, 186–200.
8. Xia, H.; Lai, M. O.; Lu, L. Nanostructured Manganese Oxide Thin Films as Electrode Material for Supercapacitors. *JOM* **2011**, *63*, 54–60.
9. Wei, W.; Cui, X.; Chen, W.; Ivey, D. G. Manganese Oxide-Based Materials as Electrochemical Supercapacitor Electrodes. *Chem. Soc. Rev.* **2011**, *40*, 1697–1721.
10. Beaudrouet, E.; Le Gal La Salle, A.; Guyomard, D. Nanostructured Manganese Dioxides: Synthesis and Properties as Supercapacitor Electrode Materials. *Electrochim. Acta* **2009**, *54*, 1240–1248.
11. Liu, R.; Duay, J.; Lee, S. B. Redox Exchange Induced MnO_2 Nanoparticle Enrichment in Poly(3,4-ethylenedioxythiophene) Nanowires for Electrochemical Energy Storage. *ACS Nano* **2010**, *4*, 4299–4307.
12. Liu, R.; Lee, S. B. MnO_2/Poly(3,4-ethylenedioxythiophene) Coaxial Nanowires by One-Step Coelectrodeposition for Electrochemical Energy Storage. *J. Am. Chem. Soc.* **2008**, *130*, 2942–2943.
13. Liu, R.; Duay, J.; Lee, S. B. Electrochemical Formation Mechanism for the Controlled Synthesis of Heterogeneous MnO_2/Poly(3,4-ethylenedioxythiophene) Nanowires. *ACS Nano* **2011**, *5*, 5608–5619.
14. Sherrill, S. A.; Duay, J.; Gui, Z.; Banerjee, P.; Rubloff, G. W.; Lee, S. B. MnO_2/TiN Heterogeneous Nanostructure Design for Electrochemical Energy Storage. *Phys. Chem. Chem. Phys.* **2011**, *13*, 15221–15226.
15. Liu, J.; Essner, J.; Li, J. Hybrid Supercapacitor Based on Coaxially Coated Manganese Oxide on Vertically Aligned Carbon Nanofiber Arrays. *Chem. Mater.* **2010**, *22*, 5022–5030.
16. Yu, G.; Hu, L.; Liu, N.; Wang, H.; Vosgueritchian, M.; Yang, Y.; Cui, Y.; Bao, Z. Enhancing the Supercapacitor Performance of Graphene/MnO_2 Nanostructured Electrodes by Conductive Wrapping. *Nano Lett.* **2011**, *11*, 4438–4442.
17. Yan, J.; Fan, Z.; Wei, T.; Qie, Z.; Wang, S.; Zhang, M. Preparation and Electrochemical Characteristics of Manganese Dioxide/Graphite Nanoplatelet Composites. *Mater. Sci. Eng., B* **2008**, *151*, 174–178.
18. Dong, X.; Shen, W.; Gu, J.; Xiong, L.; Zhu, Y.; Li, H.; Shi, J. MnO_2-Embedded-in-Mesoporous-Carbon-Wall Structure for Use as Electrochemical Capacitors. *J. Phys. Chem. B* **2006**, *110*, 6015–6019.
19. Lang, X.; Hirata, A.; Fujita, T.; Chen, M. Nanoporous Metal/Oxide Hybrid Electrodes for Electrochemical Supercapacitors. *Nat. Nanotechnol.* **2011**, *6*, 232–236.
20. Zhu, H.; Xiao, Z.; Liu, D.; Li, Y.; J. Weadock, N.; Huang, J.; Hu, L.; Fang, Z. Biodegradable Transparent Substrates for Flexible Organic-Light-Emitting Diodes. *Energy Environ. Sci.* **2013**, 10.1039/C3EE40492G .
21. Huang, J.; Zhu, H.; Chen, Y.; Preston, C.; Rohrbach, K.; Cumings, J.; Hu, L. Highly Transparent and Flexible Nanopaper Transistors. *ACS Nano* **2013**, *7*, 2106–2113.
22. Kamel, S. Pharmaceutical Significance of Cellulose: A Review. *eXPRESS Polym. Lett.* **2008**, *2*, 758–778.
23. Czaja, W.; Krystynowicz, A.; Bielecki, S.; Brown, R. M. Microbial Cellulose—The Natural Power To Heal Wounds. *Biomaterials* **2006**, *27*, 145–151.
24. Zheng, G.; Cui, Y.; Karabulut, E.; Wagberg, L.; Zhu, H.; Hu, L. Nanostructured Paper for Flexible Energy and Electronics Devices. *MRS Bull.* **2013**, *38*, 320–325.
25. He, J.; Kunitake, T.; Nakao, A. Facile *In Situ* Synthesis of Noble Metal Nanoparticles in Porous Cellulose Fibers. *Chem. Mater.* **2003**, *15*, 4401–4406.
26. Dong, A.; Wang, Y.; Tang, Y.; Ren, N. Zeolitic Tissue through Wood Cell Templating. *Adv. Mater.* **2002**, *14*, 926–929.
27. Lewin, M.; Pearce, E. M. *Handbook of Fiber Chemistry*; Marcel Dekker: New York, 1998.
28. O'Sullivan, A. Cellulose: The Structure Slowly Unravels. *Cellulose* **1997**, *4*, 173–207.
29. Topgaard, D.; Söderman, O. Diffusion of Water Absorbed in Cellulose Fibers Studied with ^{1}H-NMR. *Langmuir* **2001**, 2694–2702.
30. Li, T.-Q.; Henriksson, U.; Klason, T.; Ödberg, L. Water Diffusion in Wood Pulp Cellulose Fibers Studied by Means of the Pulsed Gradient Spin-Echo Method. *J. Colloid Interface Sci.* **1992**, *154*, 305–315.
31. Kaewprasit, C.; Hequet, E.; Abidi, N.; Gourlot, J. P. Application of Methylene Blue Adsorption to Cotton Fiber Specific Surface Area Measurement: Part I. Methodology. *J. Cotton Sci.* **1998**, *173*, 164–173.
32. Wertz, J. L.; Bédué, O.; Mercier, J. P. *Cellulose Science and Technology*; CRC Press: Boca Raton, FL, 2010.
33. Hu, L.; Pasta, M.; La Mantia, F.; Cui, L.-F.; Jeong, S.; Deshazer, H. D.; Choi, J. W.; Han, S. M.; Cui, Y. Stretchable, Porous, and Conductive Energy Textiles. *Nano Lett.* **2010**, *10*, 708–714.
34. Hu, L.; Choi, J. W.; Yang, Y.; Jeong, S.; La Mantia, F.; Cui, L.-F.; Cui, Y. Highly Conductive Paper for Energy-Storage Devices. *Proc. Natl. Acad. Sci. U.S.A.* **2009**, *106*, 21490–21494.
35. Hsu, Y.-K.; Chen, Y.-C.; Lin, Y.-G.; Chen, L.-C.; Chen, K.-H. Reversible Phase Transformation of MnO_2 Nanosheets in an Electrochemical Capacitor Investigated by *In Situ* Raman Spectroscopy. *Chem. Commun.* **2011**, *47*, 1252–1254.
36. Julien, C.; Massot, M.; Baddour-Hadjean, R.; Franger, S.; Bach, S.; Pereira-Ramos, J. P. Raman Spectra of Birnessite Manganese Dioxides. *Solid State Ionics* **2003**, *159*, 345–356.

37. Hyun, T.-S.; Kang, J.-E.; Kim, H.-G.; Hong, J.-M.; Kim, I.-D. Electrochemical Properties of MnO_x—RuO_2 Nanofiber Mats Synthesized by Co-electrospinning. *Electrochem. Solid-State Lett.* **2009**, *12*, A225–A228.
38. Bezgin, B.; Yagan, A.; Onal, A. M. Electrochemical Copolymerization of a Novel Fluorene Derivative with 3,4-Ethylenedioxythiophene. *J. Electroanal. Chem.* **2009**, *632*, 143–148.
39. Xiao, W.; Xia, H.; Fuh, J.-Y.-H.; Lu, L. Electrochemical Synthesis and Supercapacitive Properties of ε-MnO_2 with Porous/Nanoflaky Hierarchical Architectures. *J. Electrochem. Soc.* **2009**, *156*, A627–A633.
40. Lee, S. W.; Kim, J.; Chen, S.; Hammond, P. T.; Shao-Horn, Y. Carbon Nanotube/Manganese Oxide Ultrathin Film Electrodes for Electrochemical Capacitors. *ACS Nano* **2010**, *4*, 3889–3896.